EXPERIENCES IN NUMERICAL ANALYSES OF SURFACE CHARGE ON INSULATORS EXPOSED TO HIGH VOLTAGE IN VACUUM

Osamu Yamamoto

Research Institute for Applied Sciences, Kyoto University, Kyoto, Japan,
e-mail: yamakyoto@maia.eonet.ne.jp

Abstract

This paper deals with the electrical insulation of a gap bridged by a solid dielectric between a pair of electrodes in a vacuum, where the dielectric is a model of an insulating spacer holding electrodes in various vacuum devices. Such gap configuration is typical as a model for studying physical mechanisms of an electrical breakdown or a flashover in a vacuum, in which the insulation ability is considerably lower than a gap without any insulating spacers. Many researchers have long investigated the mechanisms of flashover, and it is believed that the charging of the insulator surface is the primary drive of such weakness. One of the effective approaches for studying mechanisms is to analyze the characteristic of charge accumulated on the insulator surface both by experiments and by numerical analyses. This paper reviews previous works conducted by the author's research group and demonstrates the difficulties we have encountered upon conducting the numerical analyses.

Introduction

From the engineering point of view, the insulation design against high voltages, or in high electric fields, in a vacuum is inevitable for a variety of electrical devices such as vacuum interrupters used for power switching, vacuum tubes for generating microwaves and X-rays, generators and accelerators for charged particles, and electron microscopes etc. Most of these devices consist of a pair of metal electrodes and an insulating solid dielectric for supporting the electrodes. Thus, we have to consider the insulation between the electrodes (vacuum gap) and the insulation of the solid dielectric placed between the electrodes. As the ability of bulk insulation of solid dielectrics is generally very high, the main insulation issue lies in the vacuum gap as well as the surface of the solid insulator facing the vacuum.

The mechanism of the electrical failure in vacuum gaps (discharge called as a breakdown) is different from that occurring along the surface of solids (discharge called as a surface flashover, or simply, a flashover). The breakdown voltage of a vacuum gap depends on the material of the electrodes and its surface conditions etc., for a fixed gap spacing and a voltage waveform. On the other hand, the flashover voltage along the insulator is less dependent on the electrode material, but depends heavily on the material of the insulator, its geometry, surface roughness and so on [1, 2]. The insulating capability of vacuum gaps is normally well higher than that on the surface of solids for the same spacing between the electrodes. Therefore, the present paper focuses on the surface flashover.

Several flashover mechanisms have been proposed and discussed so far [3-7]. Most of the mechanisms include charging of a surface, or a thin layer near the surface of an insulator. One of the plausible charging mechanisms relies on a phenomenon called as the secondary

electron emission avalanche (SEEA), where initial electrons are supplied by a field emission phenomenon from a cathode triple junction where the cathode, insulator and vacuum meet, or its vicinity. The electric field strength at the junction can be enhanced to $\varepsilon_r E_{av}$; ε_r as relative permittivity of the insulator and E_{av} the average electric field strength of the bridged gap. When the polarity of the surface charge is positive, it further increases the field strength and thus the amount of field-emitted electrons, which promote the progress of a SEEA. During the progress of the avalanche, electrons impinging on the insulator not only produce secondary electrons and electrify the surface, but also release gas molecules that have been adsorbed on the surface into the vacuum. The flashover is accomplished as a gas discharge in this gaseous layer [8]. Since the electrification of a surface due to a SEEA can trigger and promote the flashover, it is important to investigate the distribution of charge on the surface.

The distribution of the charge due to SEEA can be analyzed by numerically tracking the electron movement in the electric field in the vacuum, or by applying a numerical field analysis with a particular boundary condition on the insulator surface [9]. The latter is useful since we can obtain the distribution in the final state of the charging. Therefore, the paper mostly focuses on this analysis method based on our experiences.

Charging on Insulator

SEEA

With a sufficiently high electric field, the field emission of electrons occurs from a cathode triple junction or the nearby area. A portion of those electrons collides with the insulator and release secondary electrons. The secondary electron yield δ is a function of the energy A [eV] of impinging electrons as shown in Figure 1. Depending on the difference in the number of injected and released electrons, the surface acquires charge and is electrified. A part of the secondary electrons again hit on the insulator in succession, resulting in an electron avalanche (SEEA). The charge deposited on the surface due to such process is called 'SEEA charge' in this paper. The injection energy changes as the charging progresses and the secondary electron yield finally becomes unity over the surface at $A=A_1$. This condition is called an equilibrium state. Thus, the secondary electron emission yield characteristic of an insulator plays a decisive role in this theory.
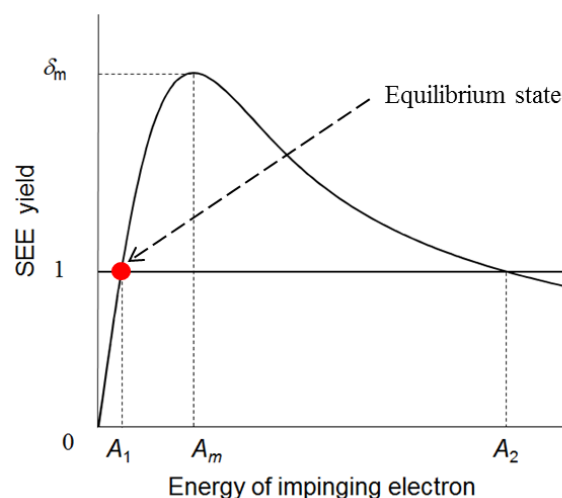
Figure 1. General characteristic of SEEA yield as a function impinging electron energy
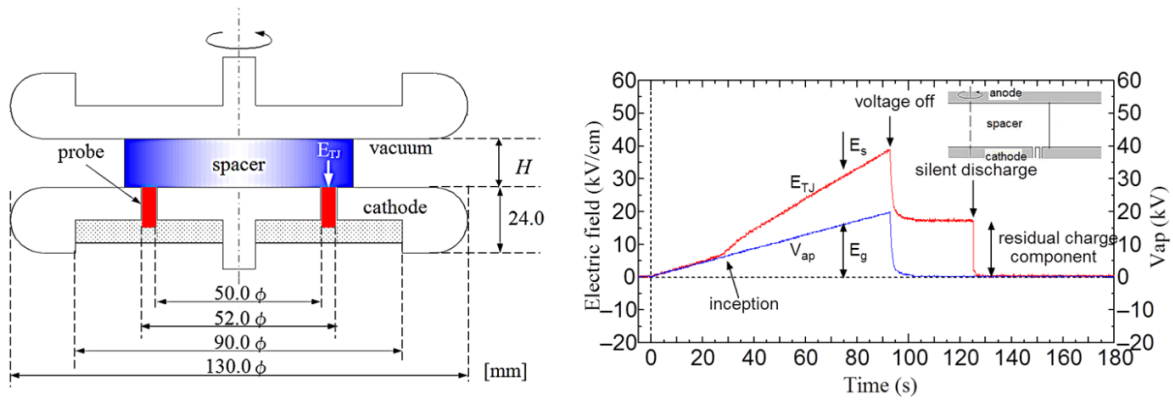
(a) gap configuration and probe arrangement   (b) applied voltage and probe signal

Figure 2. Charging phenomenon observed by an electrostatic probe [10]. (Insulator; PMMA with 54 mm radius, H= 10 mm. Pressure; 2×10^{-3} Pa.)

Figure 2 [10] shows an example of such charging phenomenon, where a pair of disc electrodes bridged by a cylindrical insulator is placed in a vacuum vessel as depicted in Figure 2a. In the experiment, the insulator was exposed to a ramped DC voltage, and then the voltage was removed before reaching the flashover event. The electric field strength on the cathode near the triple junction was measured by using a ring type electrostatic probe embedded in the cathode.

As shown in Figure 2b, the electric field consists of a geometrical field component E_g (=V_{ap}/H; V_{ap} as the applied voltage, and H the insulator length) and a SEEA charge component E_s. E_s is superimposed on E_g. The total electric field strength is denoted as E_{TJ} (=$E_g + E_s$). At a certain voltage level, the charging initiates and E_s increases almost linearly with V_{ap}. E_s remains for a long time after the voltage removal, but diminishes when a small amount of nitrogen or air is introduced in the vacuum vessel.

The charge component E_s remains since the leakage of SEEA charge is very slow because of a high resistivity of the surface. By introducing the gas in the chamber after the voltage removal, a gaseous discharge (a silent discharge) takes place due to a comparatively high electric field caused by the remaining charge at the Paschen minimum, thus the charge disappears. This phenomenon provides us a clear evidence that an insulator acquires a charge on its surface by applying a high voltage in vacuum.

Boundary Condition [11, 12]
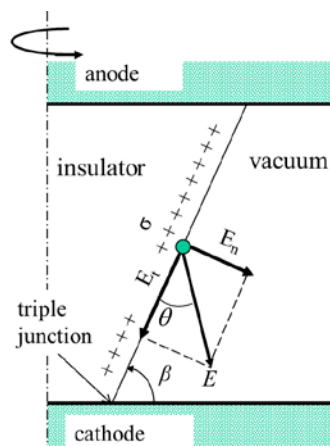
Figure 3. Explanation of normal and tangential electric fields on an angled insulator

For general applications, we take an insulator in the shape of a conical frustum with the rotationally symmetric coordinate, and its surface acquires SEEA charge at a constant density independent of the azimuth angle (See Figure 3). When the equilibrium state is reached the tangential (E_t) and normal (E_n) electric field components hold equation (1).

$$\tan\theta = \frac{E_n}{E_t} = k^{-0.5}, \qquad\qquad k = \frac{1}{2}\left(\frac{A_1}{A_s} - 1\right) \qquad\qquad (1)$$

Where, θ is the angle between E_t and E ($=E_n + E_t$), A_s the initial energy of secondary electrons and A_1 is the energy of injection electrons when the secondary electron yield $\delta=1$ (Figure 1).

Calculation Method [9]

For the SEEA charge analysis, we can employ a surface charge simulation method, which is similar to that used for static electric field calculations. The surfaces of electrodes and the insulator are subdivided into elements and each element is given an unknown charge amount. To solve the unknowns, necessary boundary conditions are;

- Potential of anode and cathode of each element on the electrodes.
- Condition of equilibrium state, i.e. Equation (1), on each element of the insulator that is expected to acquire SEEA charge.
- Condition of the electric flux continuity (div$D$=0, with D as the electric flux density)

Under these boundary conditions, we obtain simultaneous equations with unknowns, of which number equal to that of the elements. The solutions of the elements that acquire SEEA charge, however, consist of both true charge, i.e. SEEA charge, and polarization charge. The condition of the electric flux continuity is used to separate the two components.

Estimating Factor k

Difficulties exist in obtaining reliable values of A_1 and A_S in Equation (1). A_1 value might depend not only on the insulator material but also on its surface roughness, etc. Moreover, since the initial energy of secondary electrons has a bell-shaped probability distribution it is inappropriate to fix A_s as a single value. In our study, instead of using A_1 and A_s, we calculate the SEEA charge density by using a specific indicator k. To estimate the value of k, we employ an iterative method to repeatedly calculate the charge distribution and the resultant cathode electric field for different k values until the calculated electric field strength coincides with the measured one.

For example, we calculated the charge distributions for different k values as illustrated in Figure 4a. Then, the electric field on the cathode was calculated for each charge distribution
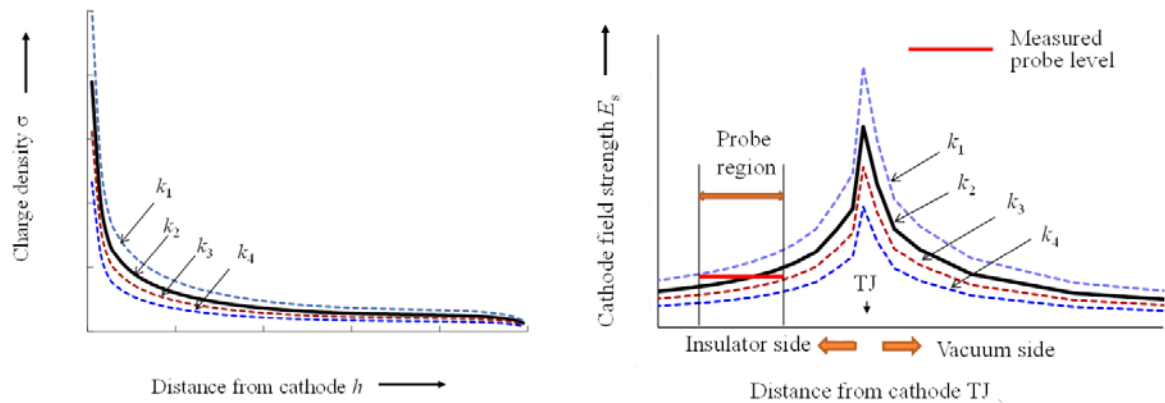
Figure 4. Schematics of calculated SEEA charge (left) and cathode electric field (right)

as shown in Figure 4b. Since the electrostatic probe was placed near the junction as shown in Figure 2a, we compared the measured field strength and the calculated ones, and selected the best-fit k value. In the estimation, we mostly used a cylindrical insulator with 50 mm height and 54mm radius.

We can successfully adopt thus estimated k value for cylindrical insulators with different lengths. We also use the same k value for different insulator shapes such as conical frustums and hollow cylinders, which are demonstrated in the subsequent sections. More details concerning the estimation method will be presented in a different paper.

Applicability of the Calculation Method

Conical Frustums [10]

Let us first define the angle of the surface of a conical frustum. We take a vertical line standing on the cathode at the triple junction, and define the angle between this line and the surface as α. When the angle between the insulator surface and the cathode surface is obtuse (See Figure 2, $90°<\beta<180°$), α is positive (Figure 5a), while α is negative (Figure 5b) when the angle is acute ($0°<\beta\leq90°$). Such an angled insulator, mostly $\alpha=+45°$, shows a high tolerance and is often adapted to a high voltage diode to support the electrode in a high power electron gun.

(a) positive angle   (b) negative angle
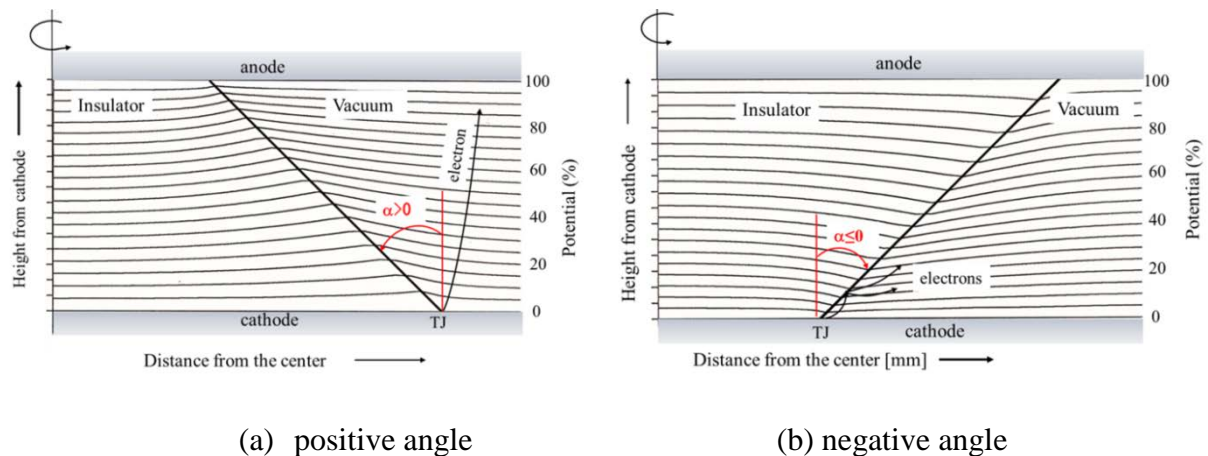
Figure 5. Definition of angle of conical frustums and the equi-potential lines

Positive Angle

For a positively angled insulator, the electric field in the vacuum directs toward the insulator surface as can be seen from the equipotential lines (Figure 5a). In such configuration, the electrons directly fly to the anode, if emitted from the triple junction, and thus the insulator surface never acquires SEEA charge. However, the computation of the SEEA charge by adopting Equation (1) yields a very high-density positive charge [9]. Furthermore, the calculation of electron trajectories assuming such positive charge on the surface has revealed that the electrons from the cathode never hit the surface. These results indicate that the result obtained by using Equation (1) is false and we cannot adopt the calculation method for positively angled frustums. This is the important point we have to take care in the charge analysis.

If the angle is very small, however, our experiment has revealed that the surface acquires a positive charge as shown in Figure 6. Thus, the limiting angle for adopting the present method exists between $0° \leq \alpha < 3°$ [10].

(a) $\alpha = 1°$ (b) $\alpha = 3°$
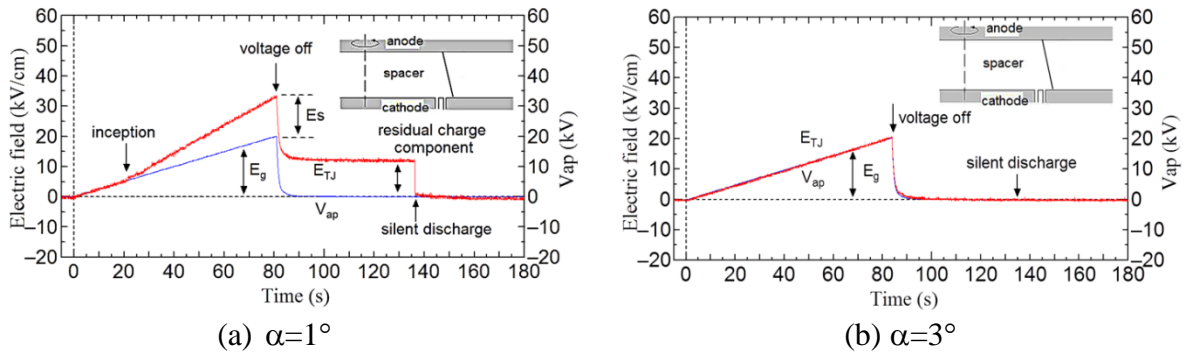
Figure 6. Probe signals for small positive angles [10]. (Insulator; PMMA, H = 10 mm)

Negative Angle

In the case of negatively angled frustums, the electric field directs toward the vacuum. Thus, the electrons from the cathode and the released secondary electrons hit the insulator (Figure 5b). Examples of SEEA charge distributions calculated for various negative angles, including a simple solid cylinder ($\alpha = 0°$), are shown in Figure 7. From the Figure, the SEEA charge density at the equilibrium state decreases as the $|\alpha|$ increases and its polarity changes from positive to negative. The polarity is positive for the angles $-20°$ $\leq \alpha \leq 0°$, and negative for $-45° \leq \alpha \leq -30°$. The turning point is around $\alpha = -25°$, at which the charge density is nearly zero.
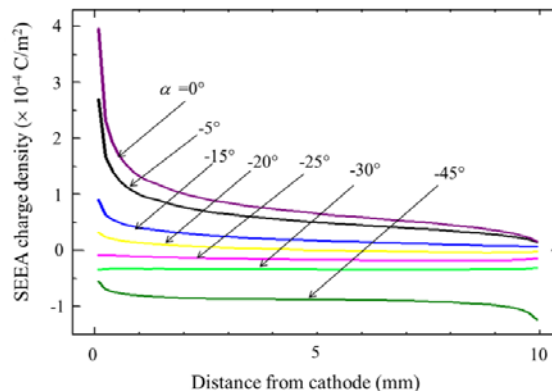
Figure 7. Calculated SEEA charge distributions for negative angles

(PMMA, H= 10 mm. k=1.56)

(a) α=-15°   (b) α=-45°
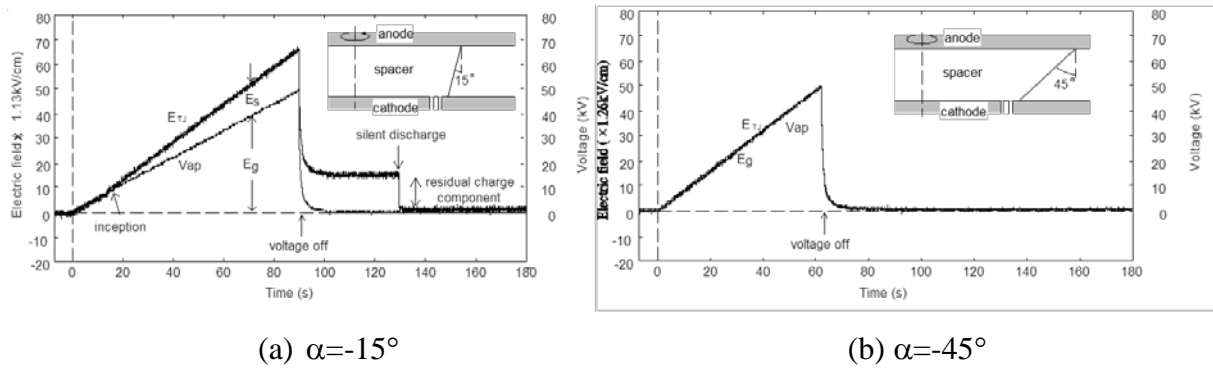
Figure 8. Probe signals for negative angles (PMMA, H=10 mm) [10]

Typical charging phenomena observed by the probe with negative angles are shown in Figure 8, where the surface is positively electrified at α=-15° (Figure 8a), but the charging does not occur at α=-45° (Figure 8b).

Figure 9 shows the measured electric field strength (E_s+E_g) normalized by E_g for each cone angle. The measurement indicates that for the positive angle (3°≤α≤45°) the normalized field strength is unity, since the surface does not acquire any SEEA charge as explained in the previous subsection. The normalized field strength is highest for α=0°, then decreases with the increase in |α| (-25°≤α<0°), and this trend coincides with that of the calculated SEEA charge (Figure 7).
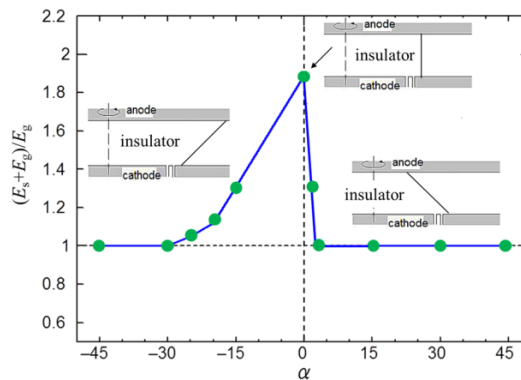
Figure 9. Measured field strength for negatively angled frustums (PMMA, H=10 mm) [10]

For more negative angles (-30°≤α≤-45°), the normalized field strength is, again, unity. This implies that such deeply angled negative frustums never acquire the SEEA charge apart from the calculation results. As a result, we conclude that the calculated charge distributions for α=-30° and -45° in Figure 7 are false. This is the second precaution when we adopt equation (1) for an insulator with angle α≤-30°.

Hollow Cylinder with a Shielding Ring [13]

A hollow type cylindrical insulator is mainly used for vacuum interrupters for AC power switching. It acts not only as a support between two electrodes but also as the vacuum vessel in which a pair of contact electrodes is installed. A metal ring, which is called as "a shielding ring" in the paper, is often furnished at each end of the cylinder to mitigate the electric field strength near the triple junction because a large potential difference appears when the contact

is opened to switch-off the power. Next experience is aimed to investigate the influence of such shielding ring on the SEEA charging.

Model of the Study
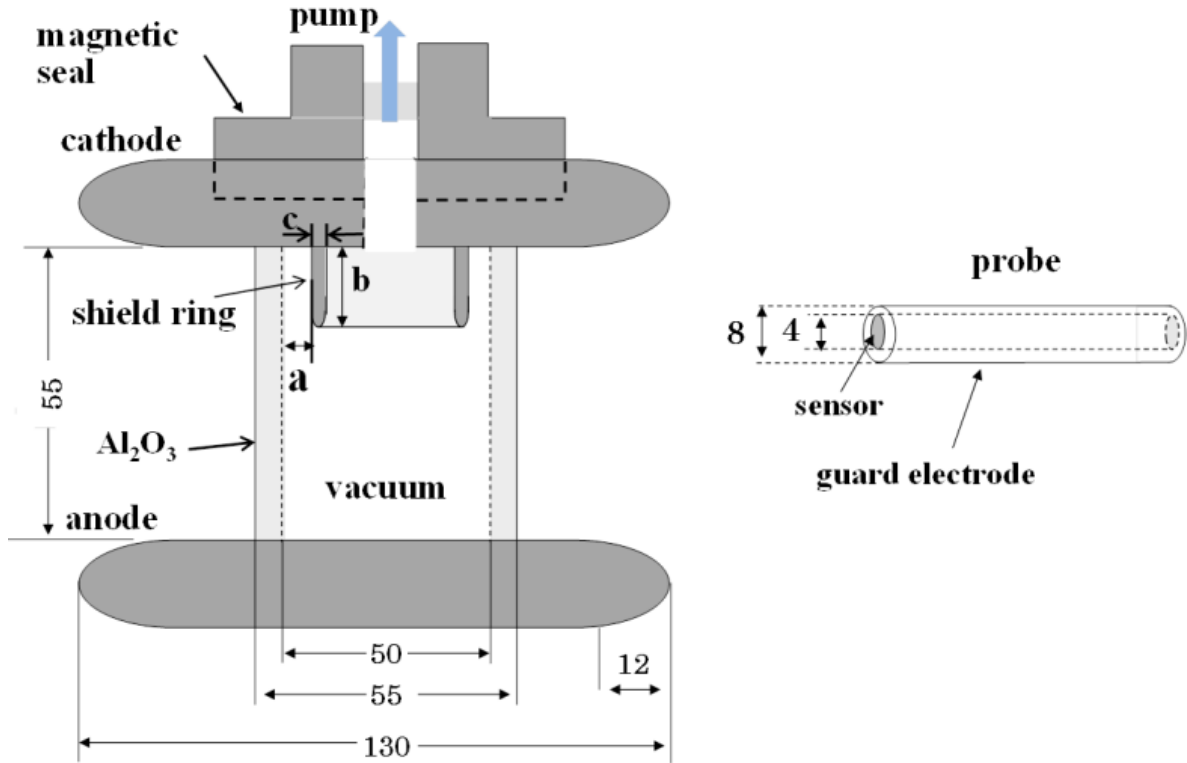
Figure 10. Gap configuration with hollow cylinder, shielding ring and probe

As described in Figure 10, the experimental system consists of an insulating hollow cylinder made of alumina (Al_2O_3, 93%), parallel electrodes and a shielding ring on the cathode, both made of aluminum. Contact electrodes and the anode side shielding ring are omitted for simplicity. To quantify the charge accumulated on the inside surface of the cylinder, an electrostatic probe is placed outside of the cylinder, at atmospheric pressure. The spacing *a* between the cylinder inner surface and the ring is fixed at 1 mm, and the height *b* of the ring from the cathode surface level is 20 mm. The top end of the ring has a curvature of 1 mm radius. The other dimensions of each part are shown in the Figure.

In the experiment, the cylinder was evacuated down to 2×10^{-3} Pa. We applied a ramped DC voltage onto the anode at an increasing rate of 2 kV/s. After the voltage reached a desired level, the voltage was kept constant for one minute. During the voltage application, the probe was kept 200 mm away from the test cylinder. After removing the voltage and grounding the anode, the probe was brought to the outer surface of the test cylinder as close as 0.8 mm. Then, the probe was moved from the cathode to the anode along the cylinder surface by using an actuator. In addition, the test specimen was rotated during the probe measurement so that the probe could scan over the whole cylinder surface from outside.

Measurement Results

Figure 11a shows the probe output pattern, where the vertical axis shows the probe output, which is obtained by dividing the induced charge on the sensor by its area. The probe output

so obtained is the charge density [μCm^{-2}]; however, this does not necessarily mean the density of true charge on the inner surface, as the probe sensor collects the electric flux from charges on different sections of the surface. Figure 11b shows the average of probe outputs for 18 circumference measurement points at the same distance from the cathode. The maximum point is at 30 mm from the cathode. This suggests that the area where the charging is depressed due to the shielding effect extends more than the height of the shielding ring [13].
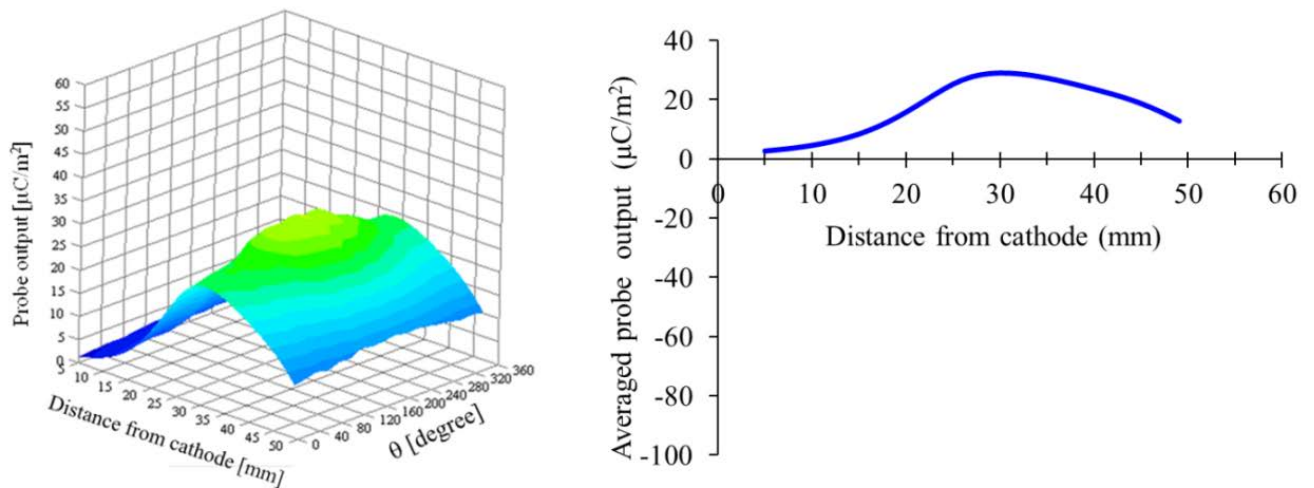
(a) original probe output   (b) averaged probe output

Figure 11. Example of probe measurement for a hollow cylinder with a shielding ring [13]

Calculation Adopting the Boundary Condition over the Inside Surface

Figure 12 shows the schematic of the gap configuration (a), calculated result of the SEEA charge in the equilibrium state (b) and calculated result of the probe output (c).

In the SEEA charge calculation, Equation (1) was adopted over the entire inner surface of the cylinder as shown in Figure 12a. To calculate the probe output, since the probe head was near to the outer surface of the cylinder during the measurement, we employed a three dimensional (3-D) calculation code delivered by CRIEPI, Japan [14]. The charge distribution in the equilibrium state (2-D distribution, Figure 12b) was given to the inner surface of the cylinder for this probe output calculation.
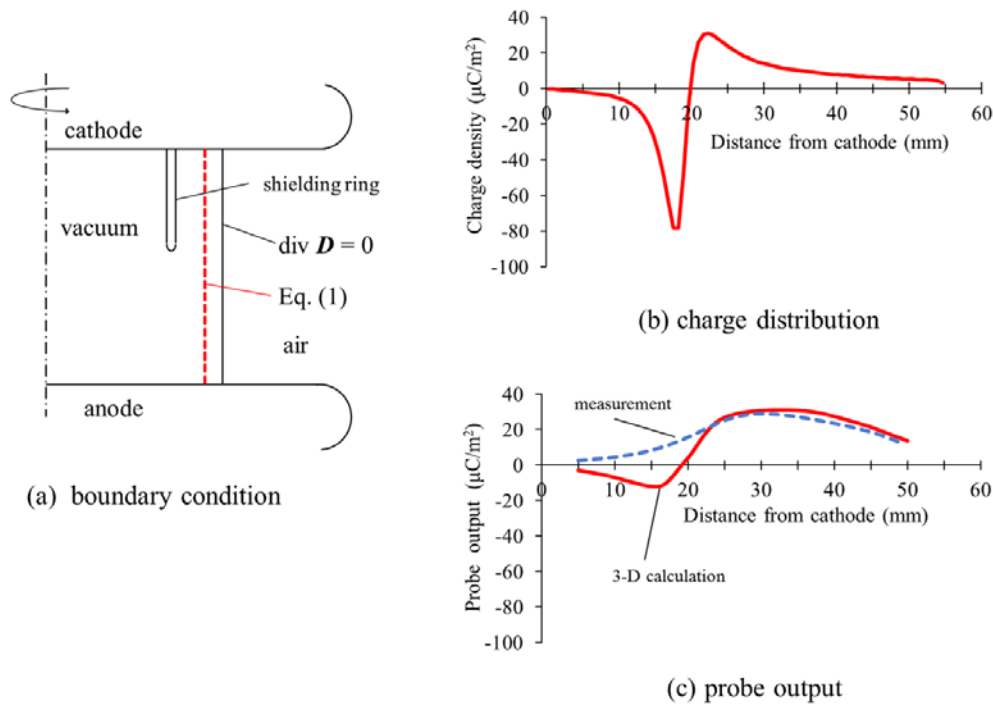
Figure 12. Calculated charge distribution and probe output [13]

As seen in the Figure 12b, the surface facing the shielding ring acquires a high-density negative SEEA charge, and the rest of the surface is positively electrified. In Figure 12c, the calculated probe output in the region facing the shielding ring is negative because it reflects the negative SEEA charge (Figure 12b).

Contrary to this calculated probe output, the measurement result does not indicate any significant negative probe signals (Figures 11a and b). So, the calculations and measurements indicate that the charging is depressed on the surface facing the shield-ring, and we can conclude that the SEEA charge distribution, especially the negative region in Figure 12b, is untrue.

Discussion and Conclusions

Negatively Angled Conical Frustums

For a negatively angled insulator with α≤-30°, the discrepancy between measured and calculated results can be caused by a small amount of negative charge accumulated at an early stage of the charging on the surface very close to the cathode, which reduces the field strength at the cathode triple junction [10]. This charge amount may be too small and localized to be detected by the probe, but large enough to cause the reduction in the field strength at the triple junction so that it suppresses the field emission of electrons to maintain an SEEA. Thus, we believe the suppression of the field emission of electrons is the cause of the zero electric field strength (E_s=0, thus normalized strength is unity) observed by the probe (Figure 8b). In fact, if we supply the electrons regardless of the field reduction, and track their trajectories, the surface acquires negative charge that coincides with the distribution in Figure 7 [9].

Influence of Shielding Ring

The study mentioned in 3.2.2 indicates that a shielding ring mitigates the charging on the insulator surface facing the ring. The reason for this result can also be attributed the depression of the field emission of electrons by a small amount of negative charge accumulated on the surface.
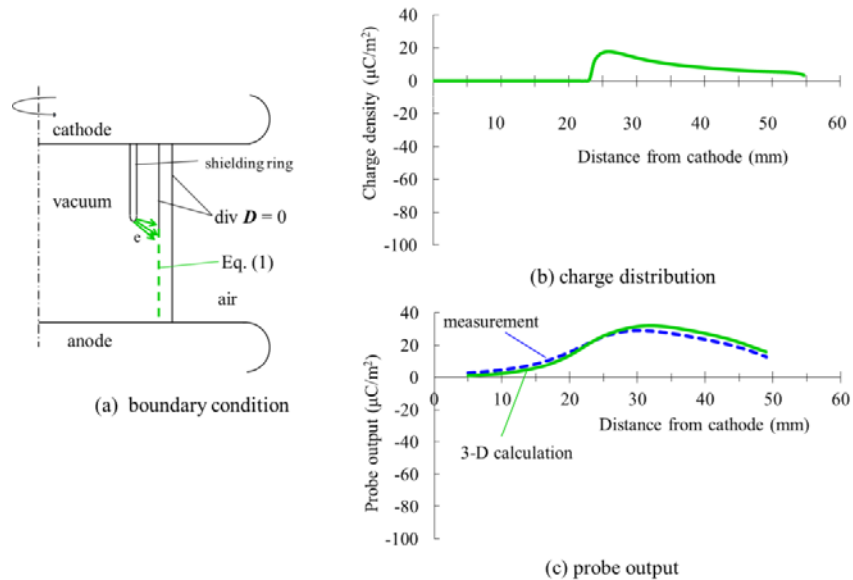
Figure 13. Calculated charge distribution and probe output [13]

Fairy good agreement is obtained between the measurement and the 3-D calculated probe output when the Equation (1) is adapted to a limited area of the inner surface. That is, the condition of continuity of electric flux (div D=0) is applied to the inner surface facing the shielding ring and some additional part extended toward the anode, while the Equation (1) is adopted on the rest of the inner surface as shown in Figure 13a. Figures 13b and 13c show these calculation results. We believe that the initial electrons are released from the shielding ring as depicted in Figure 13a.

Prospective Analyses and Necessary Data

In addition to two cases demonstrated in the present paper, the calculation results of a cylindrical insulator having ribs also showed negatively charged regions [15]. As discussed above, we must consider carefully that which part of the insulator or which insulator shape should be subjected to the boundary condition in Equation (1), particularly when a negative charge is found in the solution. We need experiences based on the experiments to obtain reasonable calculation results.

In the case when one obtains the solution showing a positive charge distribution over the targeted surface, it must be satisfactory. Even in such cases, however, it is recommended to verify the result by calculating electron trajectories as explained in 3.1.1.

To solve these key problems as a whole, it is necessary to develop a numerical calculation code that enables us a fast and precise electric field analysis in the space and on the surfaces of insulator and electrodes, especially near the cathode triple junction. This code must consider the localized surface charge during the progress of a SEEA. In conjunction with this code, we also need an additional code that enables us a fast electron trajectory analysis. Such united calculation code, together with the reliable characteristics of a secondary electron yield and of a field emission of electrons, will solve the key problems, since the field emission will

be stopped when the surface acquires a certain amount of negative charge. The field calculation and the trajectory calculation codes have been already developed [9, 16, 17], but on the way to the goal.

At the very end of this review paper, the author likes to state that an approach to solve the distribution of SEEA charge as an inverse problem based on the probe output data has been started by our international study group.

References

[1] J.B. Birks, *Progress in DIELECTRICS*, Vol. 7, Heywood Books, London, 1967.
[2] R.V. Latham, ed., *High Voltage Vacuum Engineering*, Academic Press, London, 1995.
[3] H.C. Miller, "Flashover of insulators in vacuum," *IEEE Transaction on Electrical Insulation,* Vol. 28, pp. 512-527, 1993.
[4] R.A. Anderson, "Anode-initiated surface flashover," In: *The Proceedings of the 2015 IEEE Conference on Electrical Insulation and Dielectric Phenomena (CEIDP)*, pp. 173-179, 1979.
[5] R.A. Anderson, and J.P. Brainard, "Mechanism of pulsed surface flashover involving electron-stimulated desorption," *Journal of Applied Physics*, Vol. 51, pp. 1414-21, 1980.
[6] G. Blaise, and C. Le Gressus, "Charging and flashover induced by surface polarization relaxation process," *Journal of Applied Physics*, Vol. 69, pp. 6334-39, 1991.
[7] T. Asokan, and T.S. Sudarshan, "Spectral nature of luminosity associated with the surface flashover process," *IEEE Transaction on Electrical Insulation,* Vol. 28, pp. 192-99, 1993.
[8] S. Pillai, and R. Hackam, "Surface flashover of solid dielectric in vacuum," *Journal of Applied Physics*, Vol. 53, No. 4, pp. 2983-2987, 1982.
[9] O. Yamamoto, T. Hara, I. Nakanishi, and M. Hayashi, "Monte carlo simulation of surface charge on angled insulators in vacuum," *IEEE Transaction on Electrical Insulation,* Vol. 28, pp. 706-711, 1993.
[10] O. Yamamoto, T. Takuma, Y. Kakehashi, S. Ikoma, A. Nishimoto, and T. Iida, "Charging characteristics of a conical insulating spacer in vacuum-comparison of measured and theoretical results," In: *19th International Symposium on Discharges and Electrical Insulation in Vacuum (ISDEIV)*, pp. 108-112, 2000.
[11] H. Boersch, H. Harmish, and W. Ehrlich, "Surface discharges across insulators in vacuum," *Zeitschrift für Angewandte Physik*, Vol. 15, pp. 518-525, 1963.
[12] C.H. de Tourreil, and K.D. Srivastava, "Mechanism of surface charging of high voltage insulators in vacuum," *IEEE Transaction on Electrical Insulation*, Vol. 8, No. 1, pp. 17-21, 1973.
[13] Y. Shimizu, O. Yamamoto, and H. Morii, "Control of surface charge on insulating hollow cylinder by using shield-ring in vacuum," *IEEE Transaction on Dielectrics and Electrical Insulation,* Vol. 21, No. 3, pp. 1312-1318, 2014.
[14] A. Tatematsu, and K. Tanabe, *Development of electric field calculation code using high-order element and application to evaluation of corona audible noise of electric line, CRIEPI Report*, No. H09014, 2009. (in Japanese).
[15] O. Yamamoto, T. Hara, T. Takuma, H. Matsuura, Y. Tanabe, and T. Konishi, "Numerical design of HV insulators based on charge accumulation in vacuum," *IEEE Transaction on Dielectrics and Electrical Insulation,* Vol. 4, No. 4, pp. 413-417, 1997

[16] O. Yamamoto, S. Markon, and H. Morii, "Depression of insulator charging in vacuum by partial mechanical processing," *IEEE Transaction on Dielectrics and Electrical Insulation*, Vol. 14, No. 3, pp. 606-612, 2007.

[17] T. Umemoto, Y. Shimizu, H. Naruse, and O. Yamamoto, "Three dimensional SEEA charge analyses on an insulator surface in vacuum," In: *18th International Symposium on High Voltage Engineering (ISH)*, PD-34, pp. 1053-1058, 2013.